Available online at www.sciencedirect.com
ScienceDirect
International Journal of Thermal Sciences 47 (2008) 1528–1543
International Journal of Thermal Sciences
www.elsevier.com/locate/ijts

Effect of vane/blade relative position on heat transfer characteristics in a stationary turbine blade: Part 1. Tip and shroud

Dong-Ho Rhee [a], Hyung Hee Cho [b,*]

[a] *Korea Aerospace Research Institute, Daejeon 305-333, Republic of Korea*
[b] *Department of Mechanical Engineering, Yonsei University, Seoul 120-749, Republic of Korea*

Received 10 November 2006; received in revised form 5 September 2007; accepted 12 December 2007

Available online 18 January 2008

Abstract

This study was carried out to investigate the effect of relative blade position on heat transfer in a stationary blade and shroud. A low speed wind tunnel with a single stage stationary annular turbine cascade was used. The test section is composed of sixteen guide plates and sixteen blades. The chord length of the blade is 150 mm and the mean tip clearance of the blade is 2.5% of the blade chord. Detailed mass transfer measurements were conducted for the stationary blade fixed at six different relative blade positions within a single pitch using a naphthalene sublimation method. The Reynolds number based on blade inlet velocity and chord length ranged between 1.0×10^5 and 2.3×10^5 and mean turbulence intensity was about 3%. As the blade position changed, the incoming flow field condition also changed significantly due to a blockage effect. As a result, the heat transfer on the tip and the shroud was significantly affected by the blade position because the incoming flow condition is changed. Especially, the mass transfer coefficients in the upstream region of the tip vary up to ±25% of their average values. On the shroud, the size and the level of peak regions due to flow acceleration, transition and tip leakage vortex were strongly affected by the relative blade position.

Keywords: Turbine blade; Tip; Shroud; Tip leakage flow; Heat/mass transfer; Relative position; Naphthalene sublimation method

1. Introduction

Since the turbine inlet temperature of a modern gas turbine engine has been increased steadily, the thermal load on the turbine blade, especially the tip region, is increased. In addition, the turbine blade has a finite tip clearance between the tip and the shroud and the leakage flow is generated through the clearance by the pressure difference between the pressure and suction sides of the blade. The flow entering the gap from the pressure side is accelerated, separates at the edge of the tip and then reattaches on the tip surface. Due to these flow characteristics, extremely high heat transfer rates are observed near the tip and on the tip of the blade. Also, the leakage flow discharged from the tip gap interacts with the mainstream (hot gases) near the suction side tip of the blade, which may cause excessive heat transfer on the surface. Therefore, the tip region of the turbine blade is subject to excessive thermal load and needs to be protected by intensive cooling.

The tip and near-tip regions including the shroud are difficult to cool effectively due to complicated geometry and flow patterns. Therefore, to improve the reliability and durability of the turbine blade, complex cooling techniques have been developed and used on the tip and near-tip regions. However, to obtain more effective cooling performance, a complete understanding of flow and heat transfer characteristics is required and this can be achieved by investigating detailed heat transfer characteristics on the tip and near-tip region at the same time. In addition, various operating conditions should be taken into account for an accurate analysis.

Extensive and intensive research has been performed on the heat transfer characteristics around the blade tip since the late 1990s and most studies dealing with heat transfer around the tip have used a stationary linear turbine cascade. Bunker et al. [1] and Ameri and Bunker [2] investigated tip heat transfer for different tip clearances and tip edge shapes in a linear turbine cascade. Bunker et al. [1] reviewed the studies related to tip heat

* Corresponding author. Tel.: +82 2 2123 2828; fax: +82 2 312 2159.
E-mail address: hhcho@yonsei.ac.kr (H.H. Cho).

1290-0729/$ – see front matter
doi:10.1016/j.ijthermalsci.2007.12.006

Nomenclature

C	blade chord length
C_P	static pressure coefficient
C_x	blade axial chord length
D_{naph}	diffusion coefficient of naphthalene in air
h_m	local mass transfer coefficient
l	blade span
$\dot{m}$	naphthalene mass transfer per unit time and area
p	blade pitch
P_0	total pressure of incoming flow
P_s	static pressure on blade surface or shroud
Re_C	Reynolds number based on blade chord length and incoming flow velocity
$Re_{C,ex}$	Reynolds number based on blade chord length and exit flow velocity
S	spacing between guide plate and blade
Sh_C	Sherwood number based on blade chord length
t	tip clearance
Tu	turbulence intensity of incoming flow
U	flow velocity at the vane exit
U_{mean}	average flow velocity at the guide plate exit
V_0	mean flow velocity at the inlet of the guide plate
W_1	mean flow velocity at the blade inlet
W_2	mean flow velocity at the blade exit
x, y, z, s	coordinate system (Fig. 2)

Greek symbols

α_1	guide plate exit angle
α_2	absolute flow angle at the blade exit
β_1	blade inlet angle
β_2	blade exit angle
δz	naphthalene sublimation depth
$\delta\tau$	test duration
ρ_s	solid naphthalene density
$\rho_{v,w}$	saturated vapor density of naphthalene
$\rho_{v,\infty}$	vapor density of naphthalene in the flow

transfer and suggested guidelines for further study in this field, such as consideration of blade rotation, shrouded tip geometry and tip cooling. Azad et al. [3,4] and Kwak and Han [5] have studied extensively the GE-E3 blade tip heat transfer in a stationary linear cascade using a transient liquid crystal technique. They investigated the effects of blade tip clearance (from 1 to 2.5% of blade chord), freestream turbulence intensity (6.1 and 9.7%), tip geometry and film cooling. Kwak et al. [6] investigated the effect of squealer geometry, such as single or double squealer, on heat transfer at the tip and the near-tip region and reported that different squealer geometries result in different heat transfer patterns which change the leakage flow path. The suction side squealer tip provides the lowest heat transfer coefficient at the tip and near-tip region. Saxena et al. [7,8] and Nasir [9] investigated the effects of tip geometry and unsteady wake on the tip flow and heat transfer for a blade using a steady state HSI-based liquid crystal technique. Yang et al. [10,11], Acharya et al. [12] and Saha et al. [13] studied flow and heat transfer characteristics for blades with different leakage reduction strategies including squealer tip and winglet using a commercial program, FLUENT. Jin and Goldstein [14] measured mass transfer coefficients on the flat tip of the blade in a stationary linear cascade using a naphthalene sublimation method. They changed the tip clearance from 0.86 to 6.90% of the chord for two different freestream turbulence intensities (0.2 and 12.0%). Papa et al. [15] also investigated the heat transfer characteristics on the squealer tip or the tip with winglet on the pressure side at four different tip clearances from 0.6 to 3.6% of the chord using a naphthalene sublimation method. Recently, research on film cooling in the tip region has been performed. Kwak and Han [16] studied heat transfer and film cooling on the flat and squealer tip of the blade in a linear cascade using a TLC technique. Ahn et al. [17] and Mhetras et al. [18] measured film cooling effectiveness in the tip with squealer rims using a Pressure-Sensitive Paint technique. Christophel et al. [19–21] used a two-passage linear cascade in a low speed wind tunnel to measure the heat transfer coefficient and film cooling effectiveness on the blade flat tip with dirt purge holes and film cooling holes on the pressure side surface. They found that the coolant from the pressure side holes provides an overall net heat flux reduction to the blade tip but the heat flux reduction is nearly independent of coolant flow levels. Newton et al. [22] investigated the effect of tip geometry and film cooling on the tip heat transfer for different tip clearances using a large-scale linear turbine cascade. They reported that the squealer rim reduces the heat transfer in the gap but high levels of heat transfer are found on the suction side near-tip surface where the tip leakage vortex impinges. They introduced a film cooling hole in the recirculation region on the tip and they mentioned that the high heat transfer region associated with the flow reattachment is successfully eliminated. Nasir et al. [23,24] also investigated film cooling on the tip with different tip geometries for various operating conditions using a large-scale linear cascade.

As mentioned, most of the previous studies have been conducted using a stationary linear turbine cascade with uniform incoming flow conditions. Under actual operating conditions, however, the incoming flow is not uniform and changes periodically since the blade rotates and interacts with the upstream vane periodically. This interaction includes the wake generated from the upstream vane and the incoming flow distortion. This may affect the behavior of the tip leakage flow and consequently heat transfer patterns around the blade tip. Some research [25–33] has dealt with the effect of vane/blade interaction and operating conditions on blade heat transfer and showed periodic variation in the heat transfer pattern due to the interaction.

Among the effects of vane/blade interaction, the present study focused on the effect of relative blade position. As men-

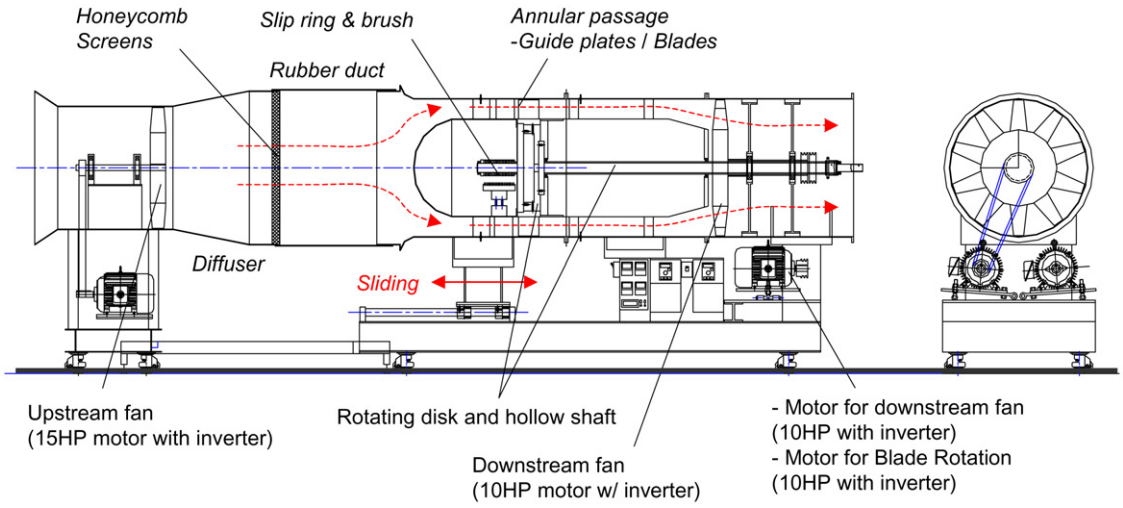

Fig. 1. Schematic view of experimental apparatus.

tioned, the relative blade position changes the opening area of the upstream vane and consequently changes the incoming flow field and heat transfer characteristics around the blade tip.

In the present study, a low speed wind tunnel with a stationary annular turbine cascade was used to study detailed heat transfer characteristics with various blade positions. The cascade has a row of guide plates in front of the stationary blade to simulate a single stage turbine. For a detailed measurement of heat/mass transfer on the blade, a naphthalene sublimation technique was used. To estimate the effect of vane/blade interaction, a set of experiments was conducted for a stationary blade with six different positions with respect to the upstream guide plate. At first, basic heat transfer characteristics were examined for uniform incoming flow conditions and then the experiments were performed on the blade fixed at various relative positions. The present study did not consider the effect of wake. To exclude the effect of upstream wake from the upstream guide vane, a thin steel plate was used to make guide vanes. In addition, the effect of Reynolds number was investigated for the condition of uniform incoming flow.

This paper presents the detailed heat/mass transfer results on the tip and the shroud for various relative positions of the blade. Part 2 presents the results on the near-tip region of the blade surface. Based on the present results, the effect of blade rotation on periodic variation of heat transfer or time-resolved heat transfer pattern with blade rotation can be estimated.

2. Experimental facilities

2.1. Wind tunnel with stationary annular cascade

Fig. 1 shows a schematic view of the low speed wind tunnel with the annular turbine cascade. The apparatus is composed of three parts: an upstream fan with 15 HP motor, an annular passage with test section (a single stage of turbine) and a downstream fan with 10 HP motor. The diffuser with a honeycomb and screens is installed at the exit of the upstream fan and connected to the annular passage by a rubber duct of 1000 mm diameter. A bell mouth and a hemispherical cone are installed at the inlet of the passage to induce a developed channel flow. The outer and inner diameters of the annular passage are 900 and 620 mm, respectively, and the corresponding height of the passage is 130 mm. The annular passage has a 1.7 m-long straight section based on the outer casing.

The test section of a single turbine stage is located in the annular passage and the cross-sectional view of the test section at the mid-span is presented in Fig. 2. To simulate a single stage turbine, the test section is designed to contain a row of sixteen guide plates in front of the stationary disk with sixteen turbine blades.

A row of the guide plates is located 540 mm downstream of the inlet of the passage. The guide plates are made of steel and their thickness is 1.3 mm. The number of guide plates is 16 and the axial chord length is 120 mm. Each guide plate has a 56.4 deg.-exit angle with a 40 mm-straight section before turning. The geometry of the guide plates is given in Table 1.

A row of turbine blades is located 34 mm downstream of the guide plate. The turbine blades are mounted on the disk, which can rotate in either direction so that the desired blade position can be obtained. The mid-span profile of GE 7FA first stage blade was used for the turbine blade. In the present study, two types of blade were used: 15 dummy blades to create a periodic flow and a naphthalene-coated test blade for local mass transfer measurement. The chord length of the blade is 150 mm and the corresponding aspect ratio is 0.87. The pitch of the blade varies from 0.84 to 1.17 in the spanwise direction and the pitch at mid-span is very close to 1.0C. The inlet and exit angles are 56.4 and −62.6 deg., respectively, which produce a turning angle of 119.0 deg. The mean tip clearance based on the measured values of the test blade is 3.8 mm, which corresponds to 2.5% of chord. It is noted that the mean tip clearance of 2.5% is somewhat larger than a typical value for an industrial gas turbine engine (1–1.5% of chord) but is reasonable to investigate the leakage flow effects on the local heat/mass transfer characteristics. The nomenclature and details of the blade geometry are given in Fig. 2 and Table 2.

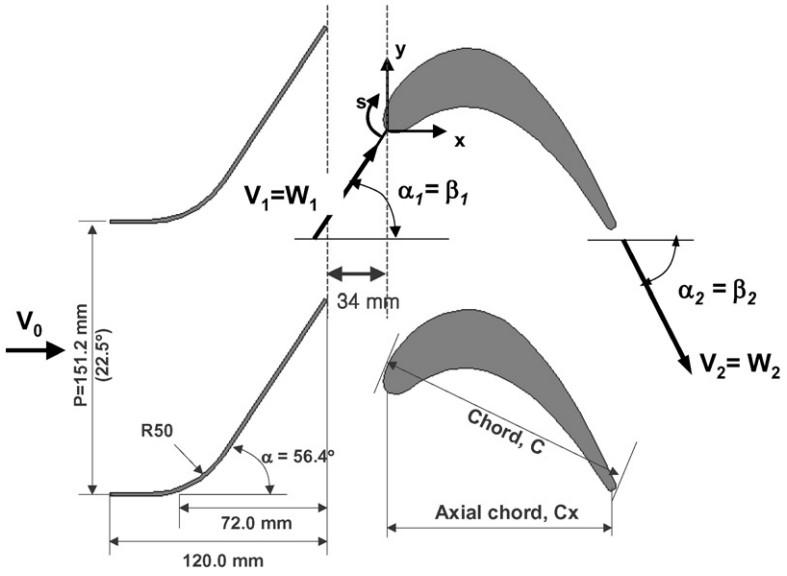

Fig. 2. Schematic view of guide vane and blade.

Table 1
Guide plate configurations

Number of guide plates	16
Axial chord length (C_x)	120 mm
Pitch	22.5°($P/C = 1.26$)
Aspect ratio (l/C)	1.08
Guide plate inlet/exit angle	0°/56.4°

Table 2
Blade configurations

Number of blades	16	
Chord length (C)	150 mm	
Axial chord (C_x)	131.5 mm	
Pitch to chord ratio (p/C)	Hub	0.84
	Mean	1.01 (22.5°)
	Tip	1.17
Aspect ratio (l/C)	0.87	
Spacing between vane and blade	34 mm (0.227C)	
Blade inlet/exit angle	$\beta_1 = 56.4°/\beta_2 = -62.6°$	
Turning angle	119.0°	
Mean tip clearance (t)	3.8 mm ($t/C = 2.5\%$)	

Two pitot tubes and six J-type thermocouples were located 100 mm upstream from the guide inlet to measure the velocity and temperature of the incoming flow. For static pressure and temperature measurements on the blade, a pressure transducer (FCO-44, Furness Controls) and J-type thermocouples with calibrated IC chips, AD594 (monolithic thermocouple amplifier with cold junction compensation, Analog Devices) were installed in the disk. The measured data were transferred to a PC through a twenty-channel slip ring in the test section.

Several windows were made on the outer casing to install the shroud test plate for local mass transfer measurements and flow/static pressure measurements. Several curvilinear test plates made of acrylic were used for velocity and static pressure measurements.

2.2. Relative position of blade and operating conditions

To investigate the effect of relative blade position, the experiments were conducted for the stationary blade fixed at six different positions. Fig. 3 shows the schematic view of the blade positions at the mid-span. The desired blade position is obtained by rotating the disk on which the blades are mounted. Position 0 (or Position 0′) means that the blade is located at the mid-way point of the passage while Position 3 means that the extended line from the guide trailing edge is coincident with the blade leading edge. Positions 1 and 2 indicate the blade positions 0.15C apart from Positions 0 and 1, respectively, in the pitchwise direction. Similarly, Positions 4 and 5 represent the positions 0.15C apart from Positions 3 and 4, respectively, in the pitchwise direction. Thus, a single pitch was resolved into six positions and the effect of blade position on local heat/mass transfer was investigated.

The experiments were conducted at the inlet Reynolds number (Re_C) of 1.5×10^5. The mean velocity at the blade inlet is 15 m/s and the turbulence intensity is about 3%. The boundary layer thickness on the casing is less than 5 mm, which is equivalent to the mean tip clearance (3.8 mm). All experiments were conducted at room temperature and the variation in room temperature during the experiments was maintained within ±0.3 °C. Details of the operating conditions are listed in Table 3.

2.3. Static pressure and flow measurements

For static pressure measurements on the blade, eleven pressure taps were fabricated at the mid-span on the dummy blades adjacent to the test blade. To measure the static pressure distribution on the shroud, a test plate with 70 pressure taps was installed. The diameter of the pressure taps is 0.8 mm for both pressure measurements.

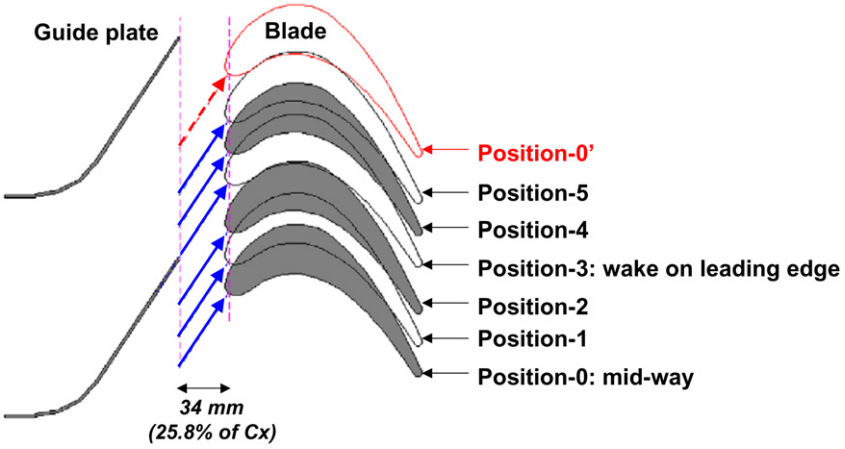

Fig. 3. Schematic of various relative positions of stationary blade.

Table 3
Operating conditions

Guide inlet flow velocity (V_0)/mean Tu	8.3 m/s/∼9%
Guide exit flow velocity (V_1)*	24.3 m/s
Blade inlet velocity (W_1)/mean Tu	15 m/s/∼3%
Blade exit velocity (W_2)*	18.0 m/s
Reynolds number based on W_1 and C($\mathrm{Re_c}$)	1.5×10^5
Reynolds number based on W_2 and C($\mathrm{Re_{C,exit}}$)	1.8×10^5

(based on mid-span geometry and the inlet Reynolds number).
* Calculated from inlet to exit area ratio.

Two pressure transducers (FCO-44, Furness Controls, Inc.) with different pressure ranges, 25 mm H_2O and 250 mm H_2O, were used. The signals from each transducer were transferred to the PC through a data logger (Model No. 34970A, Agilent Technologies, USA) with a 22 channel-multiplexer (34901A). The uncertainties of static pressure measurement were estimated as ±4.9% for the 25 mm H_2O pressure transducer and ±5.9% for the 250 mm H_2O pressure transducer.

A constant temperature thermal anemometer (IFA-300 from TSI, Inc.) with a single hot-film probe (Model 1201-6) was used to measure the boundary layer profile and the velocity and turbulence intensity of the mainflow. The sampling rate was 4000 Hz with a low pass filter at 2000 Hz and 4096 data points were acquired and averaged. Velocity magnitude and turbulence intensity distributions presented in this study were measured while the wire was positioned normal to the guide plate exit angle.

3. Mass transfer measurement and data reduction

Detailed mass transfer measurements were conducted at the blade tip and shroud using a naphthalene sublimation method. The test blade surface has a rim of 5 mm along the blade periphery of the tip to maintain the sharp edge of the blade tip and to provide a reference value for sublimation depth calculation. To measure the sublimation depth on the curved surface, four-axis positioning table with 5-phase stepping motors and LVDT depth gage (Schaevitz, LBB-375TA-020) were used. The details of the test blade and measurement system are described in Refs. [32,33].

The mass transfer coefficient is obtained from sublimation depth and exposure time. The local mass transfer coefficient is defined as follows.

$$h_m = \dot{m}/(\rho_{\mathrm{v,w}} - \rho_{\mathrm{v},\infty}) = \rho_{\mathrm{s}}(\delta y/\delta\tau)/\rho_{\mathrm{v,w}} \tag{1}$$

In the data reduction, a naphthalene concentration in the mainstream is used as a reference value and its value, $\rho_{\mathrm{v},\infty}$ is assumed to be zero in this study since freestream contains no naphthalene. The local sublimation depth (δy) is the difference between total sublimation depth and sublimation depth due to natural convection. In this study, the natural sublimation rate was determined from separate experiments and was estimated to be about 10% of the total sublimation depth. It is noted that the average total sublimation depth is less than 0.1 mm and its effect on the blade geometry variation is negligible.

The Sherwood number is expressed as:

$$\mathrm{Sh_C} = h_m C/D_{\mathrm{naph}} \tag{2}$$

where D_{naph} is calculated from a correlation equation suggested by Goldstein and Cho [34]. Uncertainty in Sherwood numbers using the method of Kline and McClintock [35] for single sample experiments was estimated to be ±7.4% in the entire operating range of the measurement, based on a 95% confidence interval. This uncertainty is mainly attributed to the uncertainty of properties of naphthalene, such as the naphthalene saturated vapor pressure (3.8%), and diffusion coefficient of naphthalene vapor in the air (5.1%).

Mass transfer coefficients can be converted into heat transfer coefficients using the heat and mass transfer analogy [36] and the comparison results for blade surface heat transfer are given by Rhee and Cho [32].

To measure the local sublimation depth on the curvilinear surface, a four-axis measurement system with an LVDT gauge was used. Detailed specifications of the measurement system are described by Rhee [37].

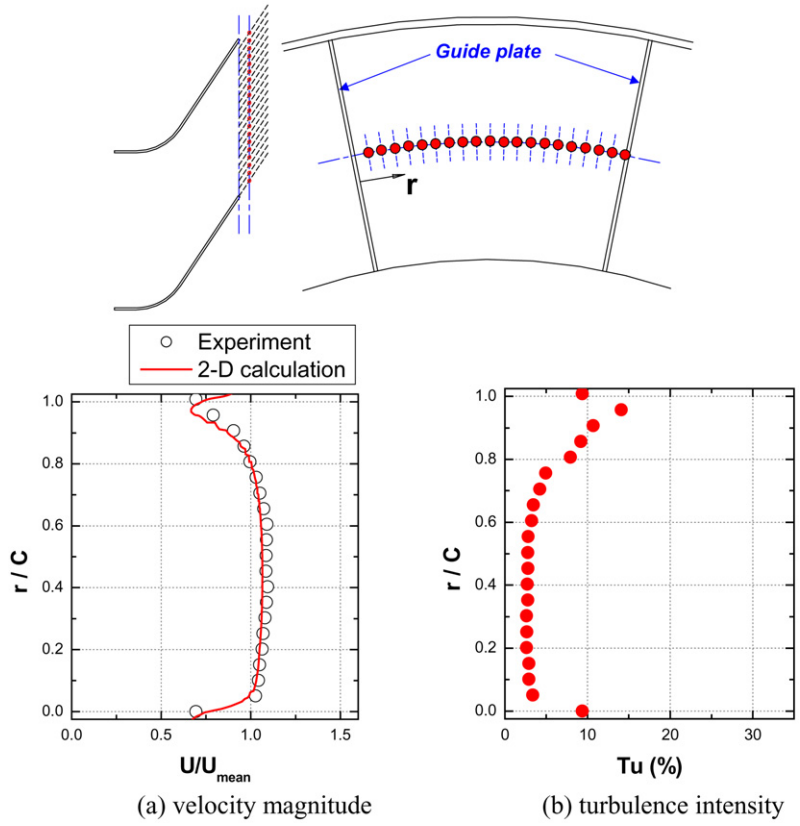

Fig. 4. Velocity magnitude and turbulence intensity at mid-span position near the guide vane exit. (a) Velocity magnitude, (b) turbulence intensity.

4. Results and discussion

4.1. Blade incoming flow measurements

Flow measurements were performed for the without blade and with blade cases at four positions (Positions 0, 2, 3 and 5) to examine the effects of the relative position on incoming flow field. Figs. 4 and 5 show the distributions of velocity magnitude and turbulence intensity at the mid-span on the plane 10 mm downstream from the guide exit. In the figures, lines refer to the results of 2D numerical simulations.

Without the blade (Fig. 4), fairly uniform distributions of velocity magnitude and turbulence intensity are obtained. The turbulence intensity at the mid-way is about 3% and it increases up to 15% at the trailing edge of the guide plate due to the wake. But the effect of this wake is relatively weak and limited in the lateral direction because a thin guide plate is used. Therefore, the effect of relative blade position on incoming flow field distribution could be investigated while the wake effect was excluded.

When the blade is installed, the blade blocks the passage and changes the flow pattern at the exit of the guide plate. This changes the flow field at the blade inlet, especially around the leading edge, as shown clearly in Fig. 5. Fig. 5 presents the distributions of velocity magnitude and turbulence intensity for the blade at four positions. In the figures, the arrow refers to the position of the leading edge of the blade.

As expected, the distributions of the velocity magnitude and turbulence intensity are quite different from those without the blade and are significantly affected by the relative position of the blade although the basic characteristics, such as low velocity and high turbulence intensity at the trailing edge regions of the guide plate, are similar.

All measurement results show low values around the blade leading edge while peak values are 25% more than the average value for all the tested cases. These low values are due to the blockage effect of the blade. Especially for Position 2, the velocity magnitude around the blade leading edge is considerably lower because the leading edge is close to the guide trailing edge. This results in an increase in turbulence intensity in the region of low velocity magnitude. Excessively high turbulence intensity is observed because of the strong flow disturbance and the wake from the guide plate and the peak value of the turbulence intensity is more than 30%. However, it should be noted that the turbulence intensity in the passage is not sensitive to the relative position. This means that other blade positions have similar patterns and levels of turbulence intensity.

Among the relative positions, Position 5 has the most uniform distributions of velocity magnitude and turbulence intensity. For this case, the difference in velocity magnitude is within $\pm 10\%$ in the passage except in the trailing edge region. Thus, the flow fields are affected significantly by the relative positions of the blade, and hence the heat transfer on the tip and the near-tip regions also is expected to be affected considerably.

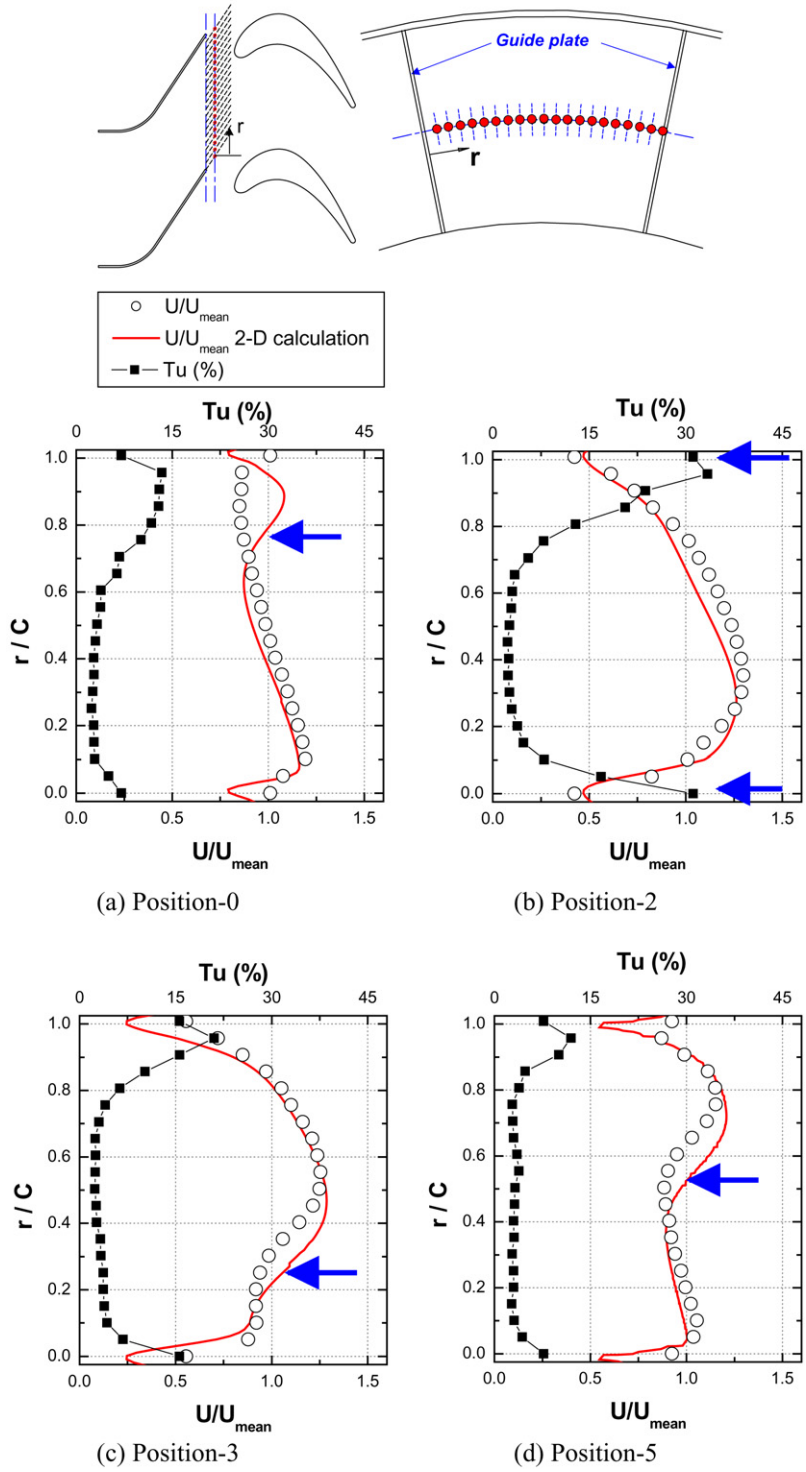

Fig. 5. Velocity magnitude distributions along the mid-span between the two adjacent guide vanes. (a) Position 0, (b) Position 2, (c) Position 3, (d) Position 5.

Fig. 6(a) shows the distributions of time-averaged static pressure coefficients at the mid-span for Position 5. Static pressure coefficient is defined in Eq. (3). It should be noted that the static pressure measurements were conducted for Position 5 because Position 5 has more uniform distribution of velocity magnitude than other cases (shown in Fig. 5).

$$C_p = (P_s - P_0)/0.5\rho V_0^2 \tag{3}$$

The bold line indicates the result from a 3D numerical simulation using FLUENT 6.1 and the open symbols represent the experimental data. The simulation was performed to obtain steady-state solutions for the turbulent viscous flow field around the blade tip. The geometry and the operating conditions are exactly the same as the experimental ones. A guide plate and a blade were modeled and a periodic boundary condition was imposed on the sidewalls. The grid was generated by

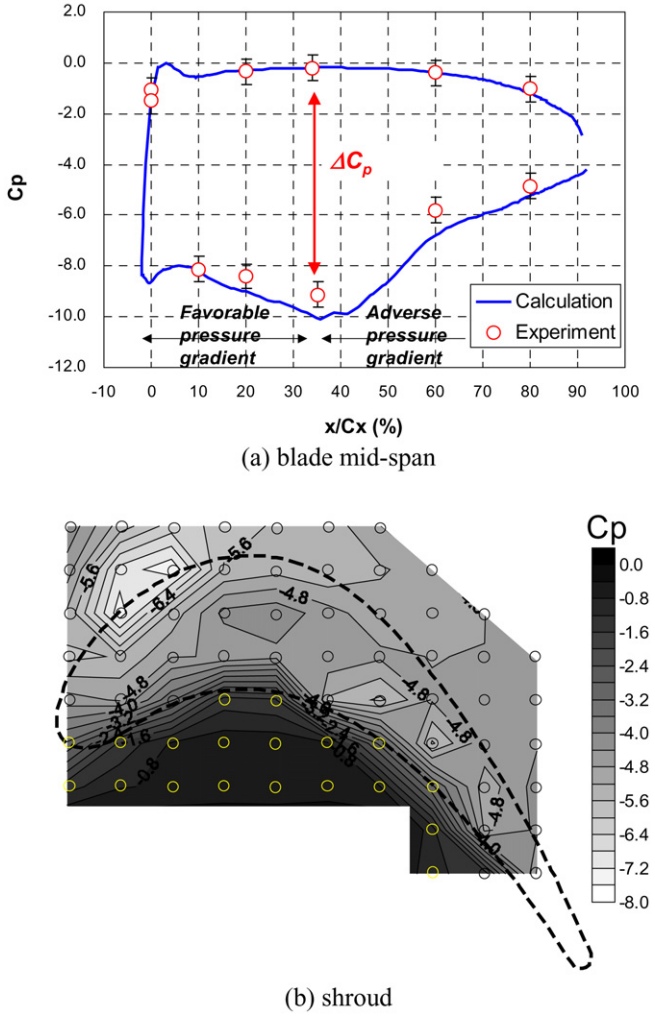

Fig. 6. Distribution of static pressure coefficients along the blade mid-span at Position 5. (a) Blade mid-span, (b) shroud.

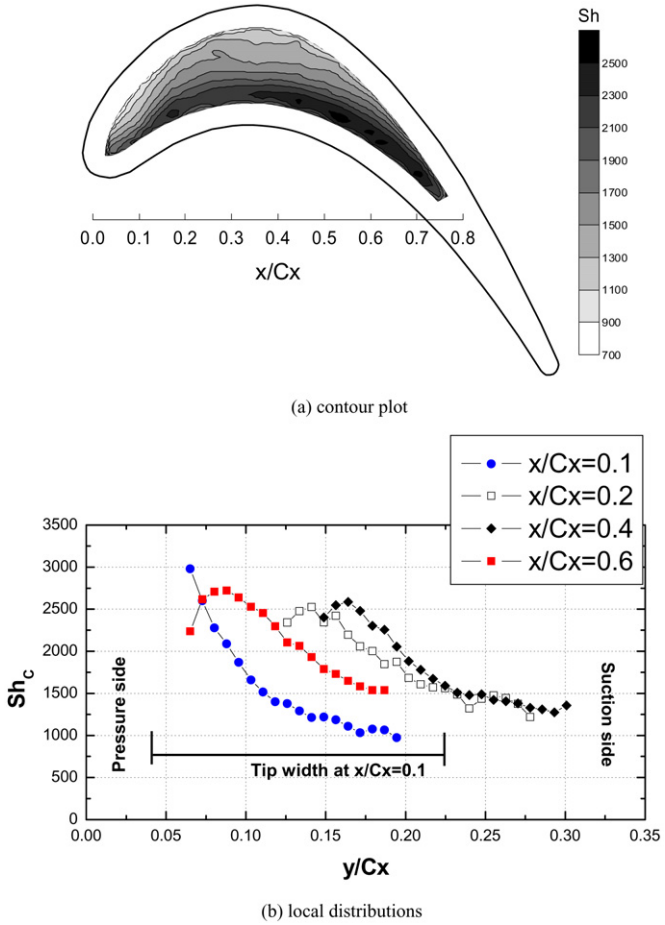

Fig. 7. Local distributions of Sh_C on the tip for Position 5 at $Re_C = 1.5 \times 10^5$. (a) Contour plot, (b) local distributions.

GAMBIT solid modeling and the number of cells was about 1.5 million. The RNG k-ε turbulence model with non-equilibrium wall function was used.

As shown in Fig. 6(a), while C_p values on the pressure side are uniform, on the suction side surface, C_p decreases considerably due to flow acceleration. The maximum static pressure difference is observed at $x/C_x \cong 0.34$ and then the static pressure recovers forming an adverse pressure gradient. Fig. 6(b) shows the measured static pressure coefficient distribution on the shroud for Position 5 at $Re_C = 1.5 \times 10^5$. In this case, the total pressure and the velocity at the inlet of the guide are used to calculate the static pressure coefficient. Small circles in the figure indicate the positions of static pressure taps. As expected in Fig. 6(a), a large difference in static pressure between the pressure and suction sides is shown along the blade periphery. The static pressure decreases sharply as the flow enters the tip clearance along the pressure side edge due to the flow acceleration (i.e. flow entrance effect). Then the static pressure decreases as the flow develops in the gap passage. Along the suction side edge, the region of the lowest coefficient at the suction side is found at $x/C_x \cong 0.15$, which corresponds to $s/C_x = 0.3 \sim 0.4$, due to the flow acceleration.

4.2. Heat/mass transfer characteristics with uniform incoming flow

Fig. 7 presents the local distributions of Sh_C on the flat tip for the stationary blade at Position 5. In the figure, the outer line and the blanked region represent the blade profile and the aluminum rim, respectively.

In the tip gap, the flow reattachment after the separation at the pressure side edge of the blade dominates the heat transfer on the tip. Therefore, the heat transfer pattern on the tip is simple: peak values at the reattachment region and then monotonic decrease with flow development. The region of high heat transfer is formed close to the pressure side edge along the pressure side in the overall region due to flow reattachment. In the upstream region, the region of high heat transfer is formed close to the pressure side edge along the pressure side while local peaks near the pressure side in the downstream region are located in the gap (approximately $0.06C_x$ from the pressure side edge) as shown in Fig. 7(b). This is because a large portion of the flow near the tip enters the gap in this region, which results in a relatively large recirculation bubble at the edge. It is noted that the

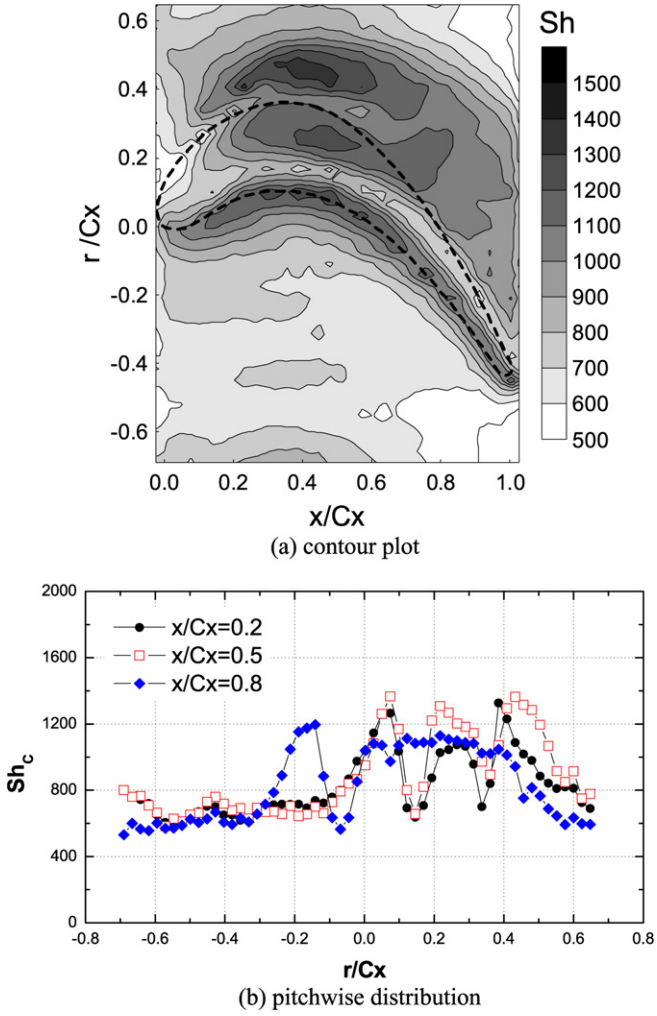

Fig. 8. Local distributions of Sh_C on the shroud for Position 5 at $Re_C = 1.5 \times 10^5$. (a) Contour plot, (b) pitchwise distribution.

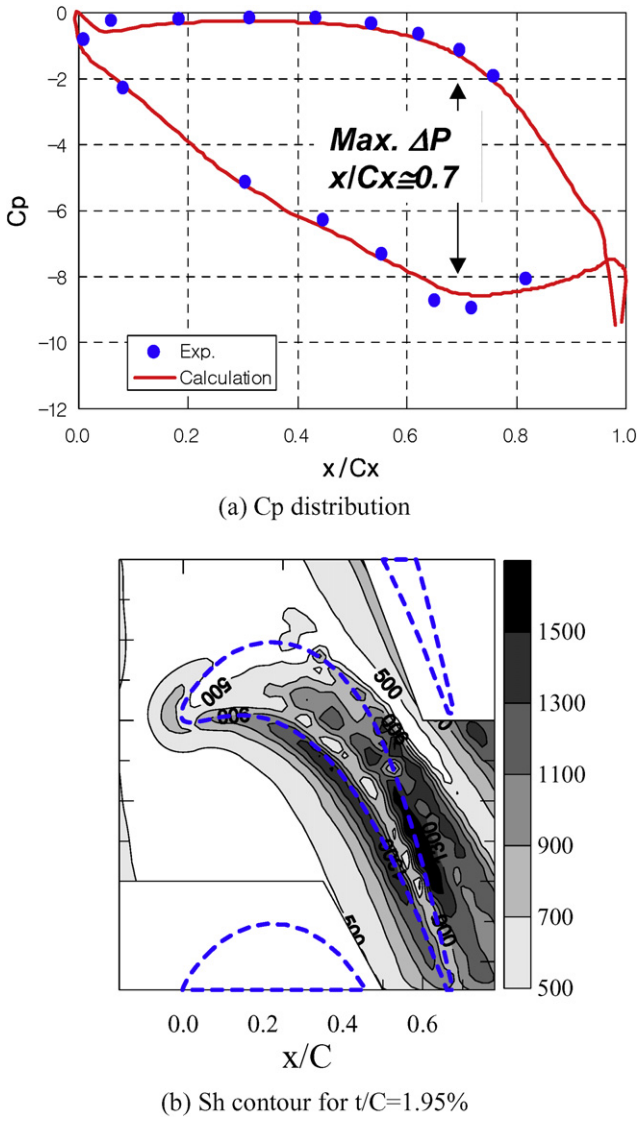

Fig. 9. Distributions of C_p at mid-span and Sh on the shroud for the blade with a low turning angle [40]. (a) C_p distribution, (b) Sh contour for $t/C = 1.95\%$.

low heat transfer region due to flow recirculation at the pressure side edge is not shown clearly because most of this region is coincident with the aluminum rim on the tip.

Relatively low transfer coefficients are observed near the suction side edge in the upstream region ($x/C_x \leqslant 0.15$). This low transfer region is in accordance with the 'sweet spot' reported by Bunker et al. [1]. This low region is formed because the tip gap flow tends to flow in the axial direction.

Local heat/mass transfer distributions on the shroud are shown in Fig. 8. While the shroud has complex heat transfer characteristics due to flow patterns such as flow acceleration, laminarization, transition to turbulent flow and leakage vortex, the overall level of heat/mass transfer coefficients on the shroud is much lower than that on the tip (about 50–70% of tip heat transfer).

As expected, locally high heat/mass transfer coefficients are observed along the pressure side because of the flow acceleration at a thin boundary layer thickness (flow entrance effect). After the flow enters the tip gap, a local valley followed by a region with peak values of heat/mass transfer coefficient is formed in the gap along the pressure side edge. These patterns are due to flow laminarization with strong flow acceleration and flow transition to turbulent flow. An additional high heat transfer region is formed outside the suction side edge due to the tip leakage flow through the upstream portion of the gap (near the leading edge). This 'upstream' tip leakage flow is thought to mainly affect the shroud after affecting the blade surface near the leading edge. Thus, the tip leakage flow seems to be divided into two streams and affects heat transfer patterns on the different regions of the blade, tip and shroud. Bindon [38] and Moore and Tilton [39] reported these flow characteristics around the tip and shroud. Also, Kwak and Han [5] and Cho et al. [40] showed a similar distribution of heat transfer coefficients, that is, additional peaks near the suction side rim on the shroud despite the different blade profile. Fig. 9 shows the pressure coefficient distribution and Sherwood number on the shroud for the blade's lower turning angle, which is presented by Cho et al. [40]. Because the turning angle is lower and the maximum pressure difference is shown in the downstream re-

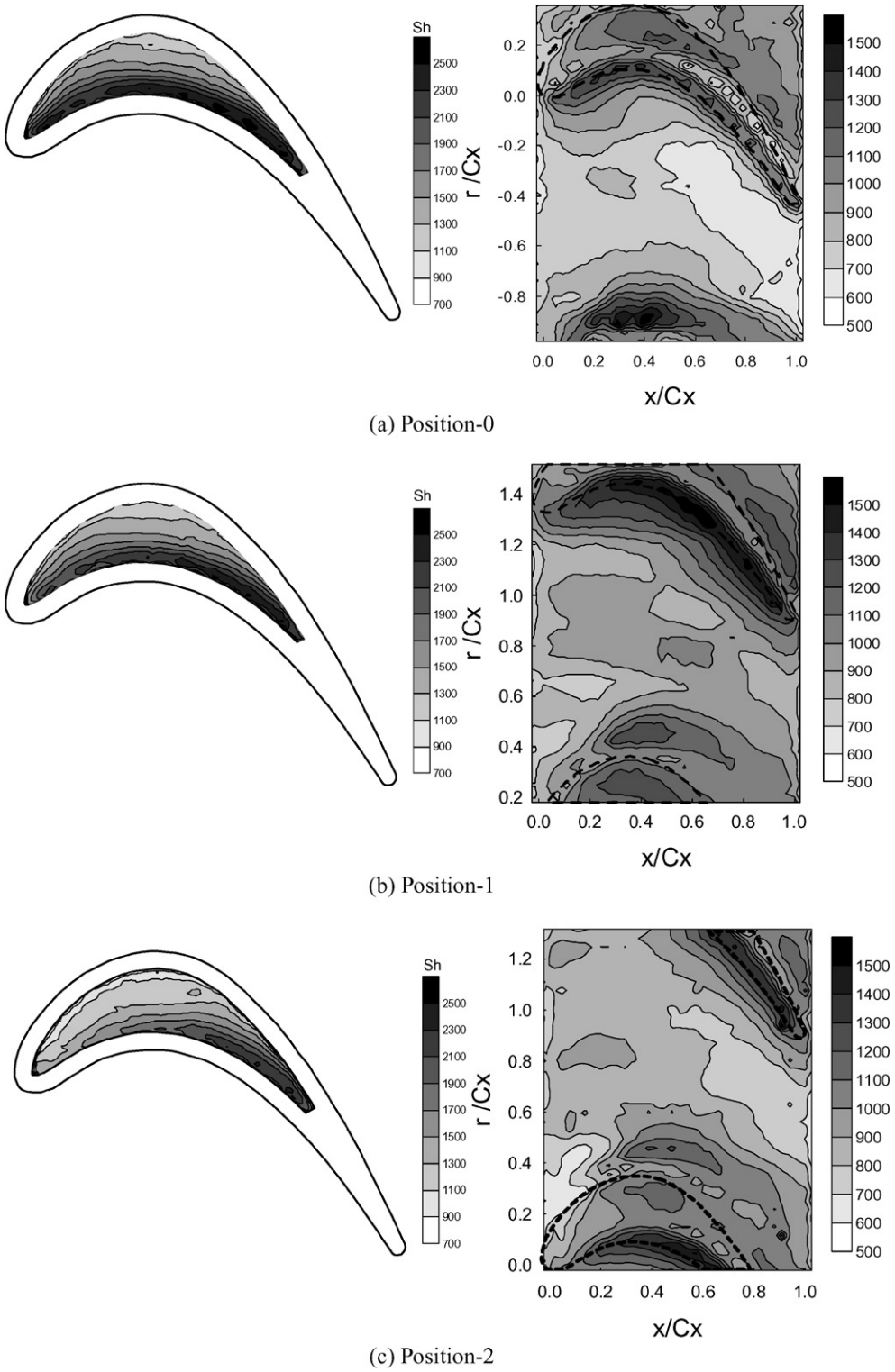

Fig. 10. Contour plots of Sh_C on the flat tip of the blade for various blade positions at $Re_C = 1.5 \times 10^5$. (a) Position 0, (b) Position 1, (c) Position 2, (d) Position 3, (e) Position 4, (f) Position 5.

gion, most tip leakage flow is driven toward the trailing edge region and the peak outside the gap is formed very close to the suction side surface. However, in the present study, this peak is formed in the upstream region and the demarcation between two peaks is clear because the blade has a higher turning angle.

The behavior of the divided tip leakage flow is discussed in detail in Part II and the details of basic heat/mass transfer characteristics on the tip and the shroud are described by Rhee and Cho [33]. The horseshoe and passage vortices are negligible in the present study because the boundary layer thickness is equivalent to the tip clearance.

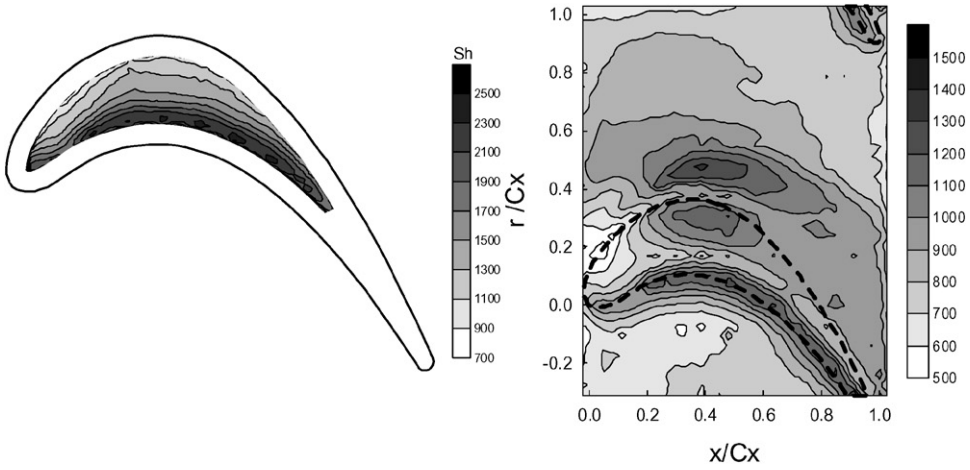

(d) Position-3

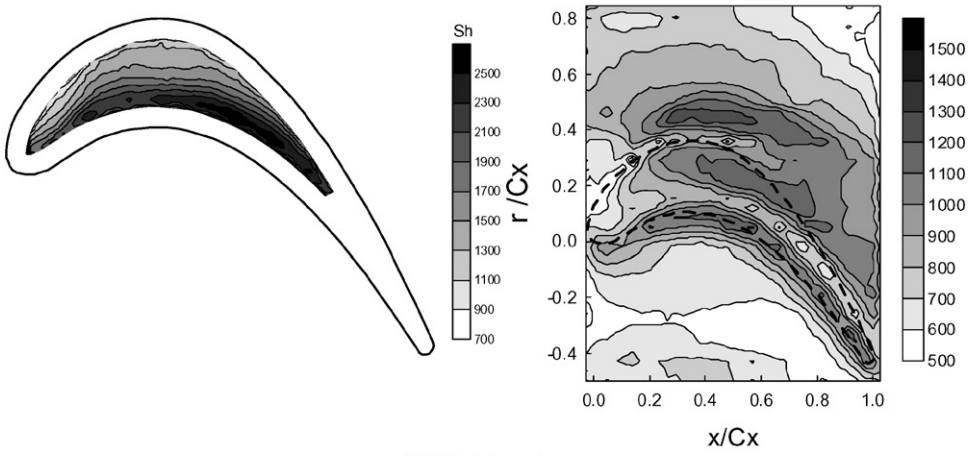

(e) Position-4

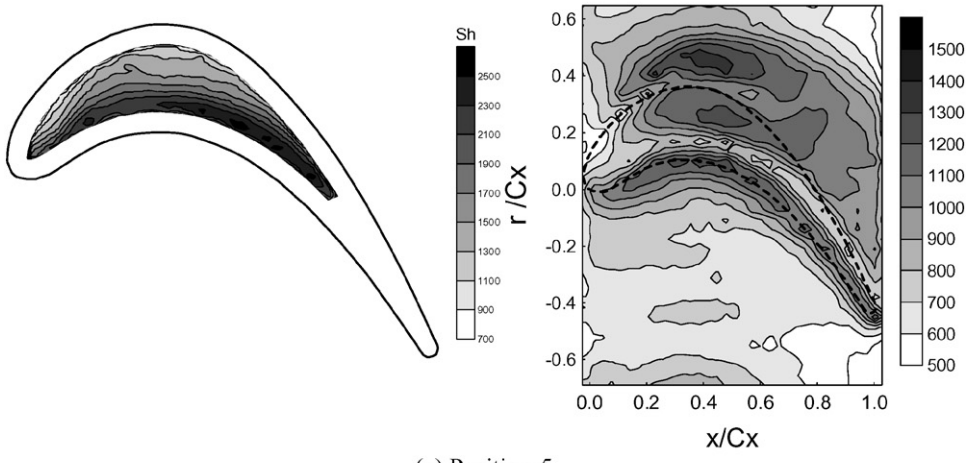

(e) Position-5

Fig. 10. Continued.

4.3. Effect of relative blade position

Fig. 10 shows the contour plots of Sh_C on the flat tip surface and the shroud for various blade positions at $Re_C = 1.5 \times 10^5$. The contours on the tip and the shroud are presented together for the same position for more exact understanding of the effect of the relative blade position. Typical heat/mass transfer characteristics are observed for all cases. But, the level of heat/mass transfer coefficients and the size of the enhanced region change. This change results from the gap flow variation, which is mentioned above, especially in the results of tip heat transfer.

At Position 0 (Fig. 10(a)), the heat/mass transfer pattern on the tip is quite similar to that at Position 5. The local Sherwood number decreases monotonically along the pitchwise direction

but its level is quite uniform along the axial direction. Local values near the leading edge (i.e. in the upstream region) are slightly higher than those at Position 5. This reveals that the portion of the upstream tip leakage flow is increased. On the shroud, the peak region outside the gap ($x/C_x \approx 0.4$ and $r/C_x \approx -0.9$) is higher than that for Position 5. This means stronger interaction between the upstream tip leakage flow and the mainflow, which results from increased upstream tip leakage flow. On the contrary, the effect of the downstream tip leakage flow, for example, peaks due to the flow transition region and the flow entrance effect is reduced when compared with the result at Position 5.

However, as the blade moves on to Positions 1 and 2, a significant change in heat/mass transfer distributions on the tip and the shroud is observed. On the tip, as shown in Figs. 10(b) and (c), the heat/mass transfer coefficients in the upstream region decrease as blade position changes to Position 2. This is because of reduction in the upstream tip leakage flow. As shown by flow measurement results, the blade inlet flow around the leading edge is disturbed and pushed toward the downstream region of the pressure side. Therefore, most of the near-tip flow is forced to enter the tip gap in the downstream portion. Those characteristics are clearly observed in the heat/mass transfer result on the shroud. High heat/mass transfer coefficients along the pressure side profile are shifted toward the downstream region, and the values are much higher than for other cases due to the increased effect of flow acceleration in this region. However, the effect of flow transition in the gap is weakened because of the shifted tip gap flow. In addition, the heat/mass transfer coefficients in the peak region outside the gap are much lower than Position 1 or 5 because of the reduced upstream tip leakage flow.

The heat/mass transfer in the passage is also influenced by the blade position. Positions 1 and 2 have higher heat/mass transfer coefficients in the passage than other cases. The reason can be inferred from the distributions of velocity magnitude. For example, the velocity magnitude in the middle of the passage is 20–25% higher than the mean value for Position 2. In other words, the incoming flow near the blade leading edge is pushed to the mid-way passage due to the blockage effect and consequently higher heat/mass transfer coefficients are observed in the passage for Position 2.

At Position 3, the mass transfer coefficients in the upstream region of the tip increase. Similarly, on the shroud surface, peak values due to the upstream tip leakage flow are higher than those for Position 1 or 2 while heat/mass transfer coefficients along the pressure side profile are lower. This is due to uniform tip gap flow over the blade periphery for Position 3.

As the blade position moves on to Position 5, the effect of the upstream tip gap flow on the shroud heat transfer becomes dominant because of the increased gap flow at these regions. Therefore, the peak region moves toward the upstream region and the level of Sherwood numbers becomes higher. However, the heat transfer patterns on the tip are similar to Position 3.

Looking over the results in series from Position 0 to Position 5 reveals that the effects of leakage flow change with the blade position and consequently the local patterns and the levels of heat/mass transfer coefficients near the tip change periodically with blade rotation. This means that the near-tip region and shroud are exposed to periodically varying heat flux. Therefore, for more accurate heat transfer analysis in the tip region of the blade, not only the uniform flow conditions but also the flow condition induced by vane–blade interaction should be considered.

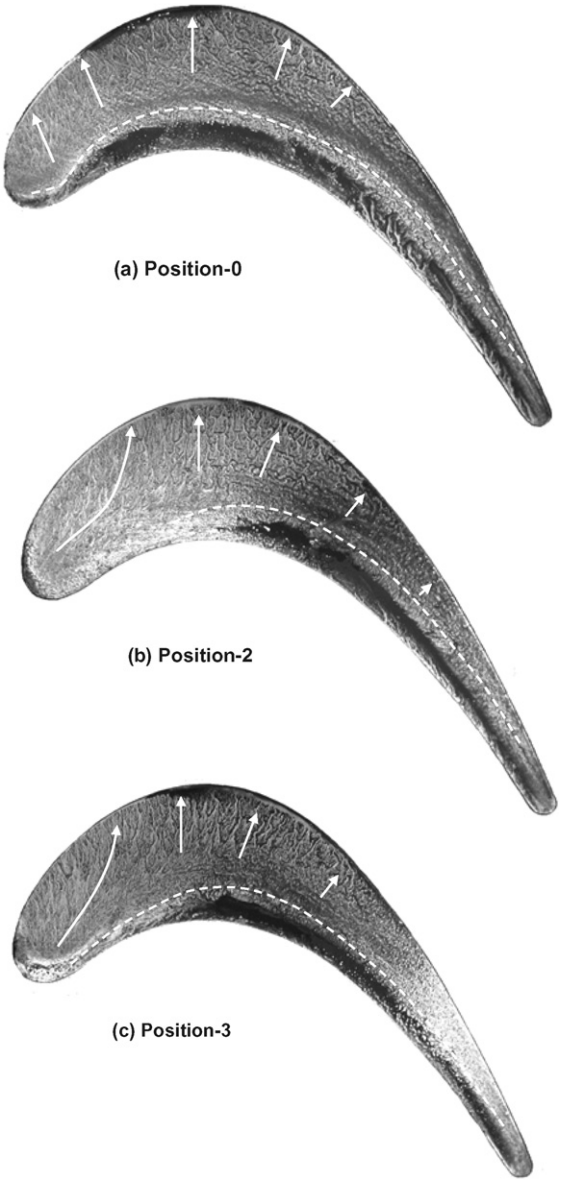

Fig. 11. Oil-lampblack flow visualization on the tip at various blade positions. (a) Position 0, (b) Position 2, (c) Position 3.

Fig. 11 shows the oil-lampblack flow visualization results for the cases at Positions 0, 2 and 3. For the visualization, the mixture of carbon powder and kerosene was used. In the figures, the dashed lines indicate the flow reattachment region along the blade and white arrows mean the expected flow direction on the tip inferred from the mass transfer experimental results and the carbon powder trajectories. These visualization results support the heat/mass transfer mechanism on the tip at various blade positions.

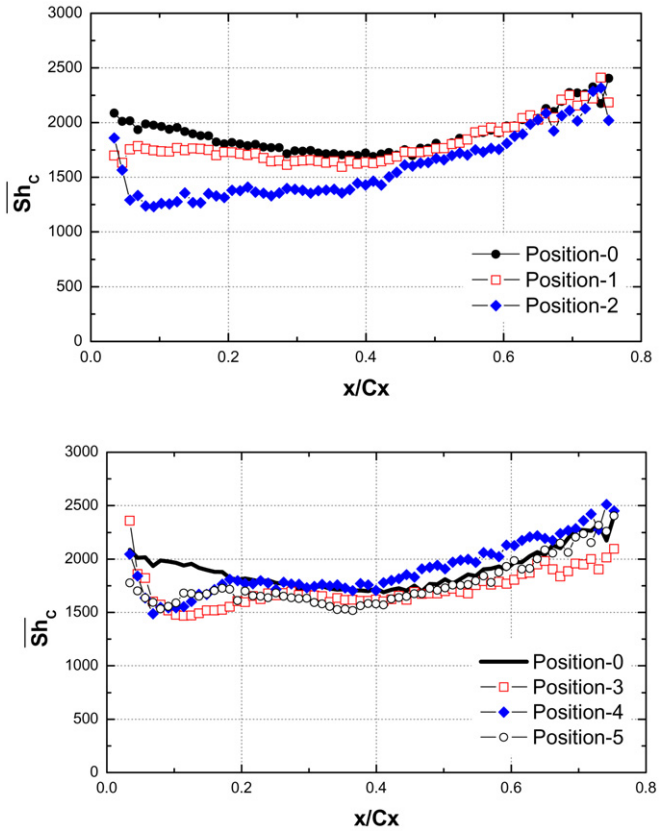

Fig. 12. Pitchwise averaged Sh_C on the flat tip of blade for various blade positions at $Re_C = 1.5 \times 10^5$.

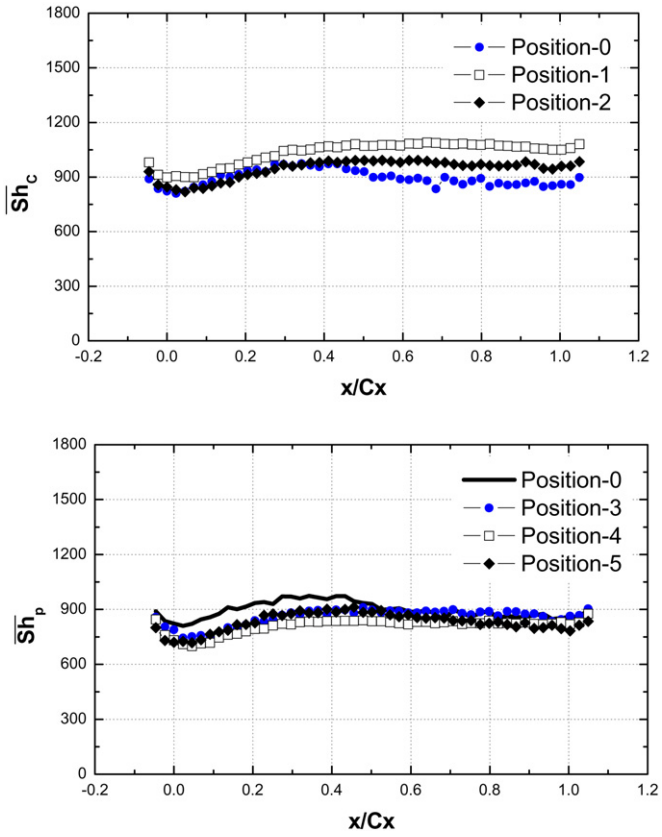

Fig. 13. Pitchwise averaged Sh_C on the shroud surface for various blade positions at $Re_C = 1.5 \times 10^5$.

Figs. 12 and 13 present the pitchwise averaged Sh_C on the tip and the shroud for various blade positions. On the tip, significant variation of Sh_C is found in the upstream region with changing blade position. Position 2 has the lowest values and the level of Sh_C is 50–80% of that at Position 0 or 5. As mentioned, this is because most of the tip gap entering flow is pushed to the downstream region for Position 2. However, the elevated turbulence intensity of mainflow does not seem to have a noticeable effect on tip heat transfer. Unlike the upstream region, the downstream region has a similar level of Sh_C because flow reattachment dominates heat transfer as shown in Fig. 11. Thus, the heat transfer in the upstream region of the tip is significantly affected by vane–blade interaction and the periodic variation of heat transfer coefficients is expected for the rotating blade.

On the shroud, although the local distributions are non-uniform and change with the variation of the blade position, the average values are almost the same. Positions 1 and 2 have slightly higher average values than other cases due to the increased heat/mass transfer rate along the pressure side edge in the passage.

Total averaged Sh_C values are presented in Fig. 14. It is noted that the average value on the shroud is only 50–70% of the values on the tip. On the tip, as shown in the local and pitchwise averaged Sh_C distributions, the value at Position 2 is the lowest and a sinusoidal pattern is observed with changing position, which is similar to the ΔC_p distribution. On the contrary,

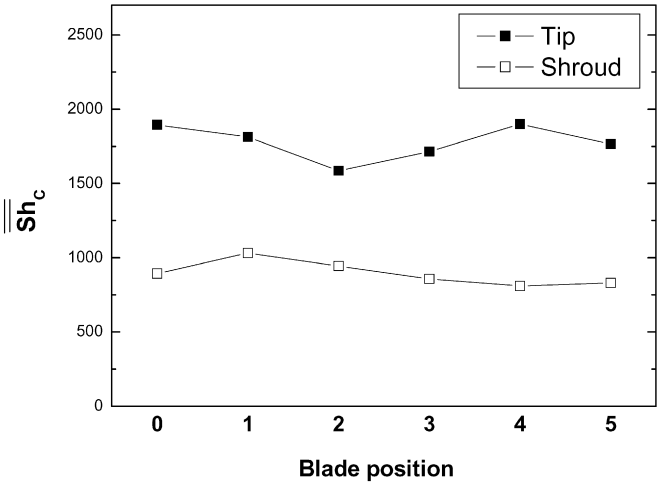

Fig. 14. Total average Sh_C on the tip and the shroud surface at $Re_C = 1.5 \times 10^5$.

average mass transfer coefficient on the shroud is not quite affected by the relative position of the blade. Although Position 1 shows a higher value than other cases, the differences between the averaged values are within the experimental uncertainty.

4.4. *Effect of Reynolds number*

To examine the effect of Reynolds number on the tip and shroud heat transfer, the experiments were carried out for various inlet Reynolds numbers ranging from 1.0×10^5 to

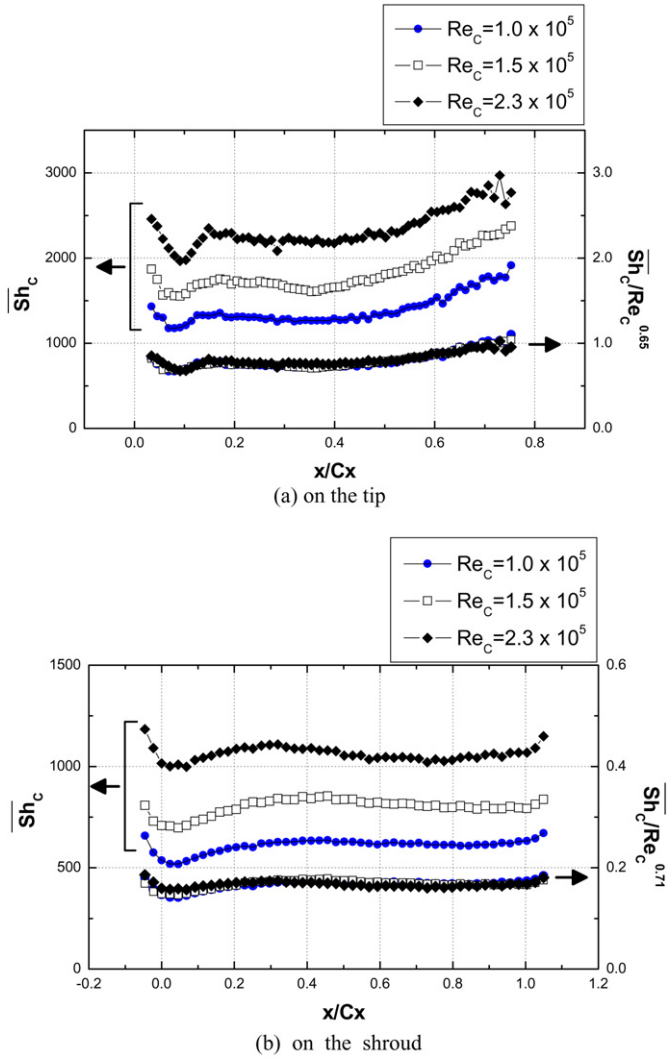

Fig. 15. Pitchwise averaged Sh_C on the tip and the shroud for Position 5 at various Reynolds numbers. (a) On the tip, (b) on the shroud.

2.3×10^5. Fig. 15 shows the streamwise distributions of pitchwise averaged Sh_C on the tip and the shroud for various inlet Reynolds numbers. The total averaged Sh_C is presented in Fig. 16.

As shown in Fig. 15(a), the levels of Sh_C on the tip increase with increasing Reynolds number while the patterns are the same. When the gap flow is fully turbulent, heat transfer on the tip can be normalized by $Re^{0.8}$ (based on the channel height) as reported by Moore and Tilton [38] because the tip gap flow can be simplified as the flow in a channel of small height. However, the exponent of the denominator (Re^n) may be different from that for the channel flow ($n = 0.8$) since the tip gap has very complex flow patterns including flow separation and reattachment at the pressure side edge. The pitchwise averaged Sh_C values normalized by $Re_C^{0.65}$ are also plotted in Fig. 15(a). The results show that pitchwise averaged values converge into a single curve. This reveals that the simplification to the channel flow has a limitation since the tip gap has complex flow patterns, such as flow separation and reattachment.

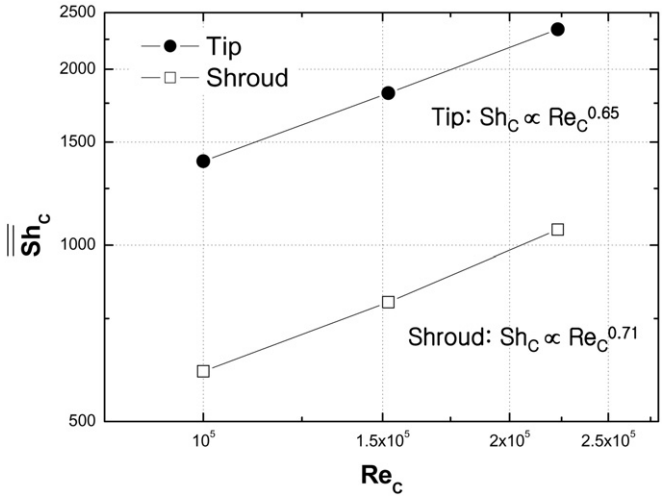

Fig. 16. Total average Sh_C on the flat tip of blade and shroud.

Heat/mass transfer distributions on the shroud also have the same trends, as shown in Fig. 15(b). The overall heat/mass transfer increases with increasing Reynolds number. For the heat transfer on the shroud, the heat/mass transfer coefficients can be normalized by $Re_C^{0.71}$ and the normalized values are coincident with each other. Like tip heat transfer, shroud heat transfer is less dependent on Reynolds number than on simple turbulent flow since the shroud also has complex flow patterns such as flow acceleration, laminarization, transition and leakage vortex near the surface.

5. Conclusions

The experimental study was conducted to investigate the effect of relative position of a stationary blade on blade tip and shroud heat/mass transfer. Detailed heat/mass transfer coefficients were obtained using a naphthalene sublimation method. The results are summarized as follows.

With uniform incoming flow, flow reattachment dominates the tip heat transfer and a high heat/mass transfer region is formed along the pressure side edge. Then, the mass transfer coefficient decreases gradually as the tip gap flow develops in the gap. On the shroud, complex heat transfer patterns are observed due to flow acceleration, relaminarization, transition to turbulent flow and tip leakage vortex. Especially, tip leakage flow is divided into two streams and each leakage flow affects local heat transfer on the shroud outside the gap and in the tip, respectively.

The relative position of the blade changes the incoming flow condition significantly because the opening area varies with the relative position. Therefore, velocity magnitude and turbulence intensity at the blade inlet change significantly with the blade position. Especially at Positions 1 and 2, most of the incoming flow is pushed to the downstream region of the pressure side and turbulence intensity around the leading edge is extremely high due to a strong blockage effect. Position 5 shows the most uniform velocity and turbulence intensity distributions.

The heat/mass transfer pattern on the tip is significantly affected by the blade position. Especially, the variation in the

heat/mass transfer coefficients in the upstream region of the tip reaches up to ±25% of the average value. For example, Position 2 has 50% lower values than Position 0 or 5 in the upstream region. However, the downstream region is hardly affected because flow reattachment dominates the heat transfer. Therefore, for the actual operating condition, the upstream region of the blade tip is possibly exposed to a periodically varying thermal load. On the shroud, like the tip, local distributions of the heat/mass transfer coefficients are affected by the relative position of the blade. As the blade position moves from Position 0 to Positions 1 and 2, the heat/mass transfer coefficients along the pressure side gap increase significantly while the peak region outside the gap near the suction side surface is reduced because the tip gap entering flow is pushed to the downstream region. Positions 3 to 5 show similar patterns to Position 0 although the level of Sh and the size of the peak regions vary with blade position change. Thus, the variation in the blade position causes the heat transfer variations and consequently, this might result in deterioration of durability in the tip region for the actual operation

The heat/mass transfer on the tip and the shroud is proportional to $Re_C^{0.65}$ and $Re_C^{0.71}$, respectively. This means that the heat transfer on the tip and the shroud is less dependent on the Reynolds number than the case for turbulent flow in a channel ($Re_C^{0.8}$) and this is mainly due to complex flow patterns such as flow separation, reattachment, relaminarization and flow transition.

References

[1] R.S. Bunker, J.C. Bailey, A.A. Ameri, Heat transfer and flow on the first stage blade tip of a power generation gas turbine. Part 1: Experimental results, ASME Journal of Turbomachinery 122 (1999) 263–271.

[2] A.A. Ameri, R.S. Bunker, Heat transfer and flow on the first stage blade tip of a power generation gas turbine. Part 1: Simulation results, ASME Journal of Turbomachinery 122 (1999) 272–277.

[3] G.S. Azad, J.C. Han, S. Teng, R.J. Boyle, Heat transfer and pressure distributions on a gas turbine blade tip, ASME Paper No. 2000-GT-194, 2000.

[4] G.S. Azad, J.C. Han, R.J. Boyle, Heat transfer and flow on the Squealer tip of a gas turbine blade, ASME Paper No. 2000-GT-195, 2000.

[5] J.S. Kwak, J.C. Han, Heat transfer coefficients on the squealer tip and near squealer tip regions of a gas turbine blade, ASME Journal of Heat Transfer 125 (2003) 669–677.

[6] J.S. Kwak, J.Y. Ahn, J.C. Han, C.P. Lee, R.S. Bunker, R. Boyle, R. Gaugler, Heat transfer coefficients on the squealer tip and near tip regions of a gas turbine blade with single or double squealer, ASME Paper No. GT2003-38907, 2003.

[7] V. Saxena, H. Nasir, S.V. Ekkad, Effect of blade tip geometry on tip flow and heat transfer for a blade in a low speed cascade, ASME Journal of Turbomachinery 126 (2003) 130–138.

[8] V. Saxena, S.V. Ekkad, Effect of squealer geometry on tip flow and heat transfer for a blade in a low-speed cascade, ASME Journal of Heat Transfer 126 (2004) 546–553.

[9] H. Nasir, S.V. Ekkad, D. Kontrovitz, R.S. Bunker, C. Prakash, Effect of tip gap and squealer geometry on detailed heat transfer measurements over a HPT turbine blade tip, ASME Journal of Turbomachinery 126 (2004) 221–228.

[10] H. Yang, S. Acharya, S.V. Ekkad, C. Prakash, R.S. Bunker, Flow and heat transfer predictions for a flat-tip turbine blade, ASME Paper No. GT2002-30190, 2002.

[11] H. Yang, S. Acharya, S.V. Ekkad, C. Prakash, R.S. Bunker, Numerical simulation of flow and heat transfer past a turbine blade with a squealer-tip, ASME Paper No. GT2002-30193, 2002.

[12] S. Acharya, H. Yang, S.V. Ekkad, C. Prakash, R.S. Bunker, Numerical study of flow and heat transfer on a blade tip with different leakage reduction strategies, ASME Paper No. GT2003-38617, 2003.

[13] A.K. Saha, S. Acharya, C. Prakash, R.S. Bunker, Blade tip leakage flow and heat transfer with pressure side winglet, ASME Paper No. GT2003-38620, 2003.

[14] P. Jin, R.J. Goldstein, Local mass/heat transfer on a turbine blade tip, in: 9th International Symposium on Transport Phenomena and Dynamics of Rotating Machinery, Hawaii, USA, Paper No. HT-ABS-012, 2002.

[15] M. Papa, R.J. Goldstein, F. Gori, Effects of tip geometry and tip clearance on the mass/heat transfer from a large-scale gas turbine blade, ASME Journal of Turbomachinery 125 (2003) 90–96.

[16] J.S. Kwak, J.C. Han, Heat transfer coefficients and film-cooling effectiveness on a gas turbine blade tip, ASME Journal of Heat Transfer 125 (2003) 494–502.

[17] J.Y. Ahn, S. Mhetras, J.C. Han, Film-cooling effectiveness on a gas turbine blade tip using pressure sensitive paint, ASME Paper No. GT2004-53249, 2004.

[18] S. Mhetras, H. Yang, Z. Gao, J.C. Han, Film-cooling effectiveness on squealer rim walls and squealer cavity floor of a gas turbine blade tip using pressure sensitive paint, ASME Paper No. GT2005-68387, 2005.

[19] J.R. Christophel, K.A. Thole, F.J. Cunha, Measured adiabatic effectiveness and heat transfer for blowing from the tip of a turbine blade, ASME Paper No. GT2004-53250, 2004.

[20] J.R. Christophel, K.A. Thole, F.J. Cunha, Cooling the tip of a turbine blade using pressure side holes. Part 1: Adiabatic effectiveness measurements, ASME Paper No. GT2004-53251, 2004.

[21] J.R. Christophel, K.A. Thole, F.J. Cunha, Cooling the tip of a turbine blade using pressure side holes. Part 2: Heat transfer measurements, ASME Paper No. GT2004-53254, 2004.

[22] P.J. Newton, S.K. Krishnababu, G.D. Lock, H.P. Hodson, W.N. Dawes, J. Hannis, C. Whitney, Heat transfer and aerodynamics of turbine blade tips in a linear cascade, ASME Paper No. GT2005-69034, 2005.

[23] H. Nasir, S.V. Ekkad, R.S. Bunker, C. Prakash, Effects of tip gap film injection from plain and squealer blade tips, ASME Paper No. GT2004-53455, 2004.

[24] H. Nasir, S.V. Ekkad, R.S. Bunker, Effect of tip and pressure side coolant injection on heat transfer distributions for a plane and recessed tip, ASME Paper No. GT2005-68595, 2005.

[25] G.R. Guenette, A.H. Epstein, R.J.G. Norton, C. Yuzhang, Time resolved measurements of a turbine rotor stationary tip casing pressure and heat transfer field, AIAA Paper No. 85-1220, 1985.

[26] G.R. Guenette, A.H. Epstein, M.B. Giles, R. Haimes, R.J.G. Norton, Fully scaled transonic turbine rotor heat transfer measurements, ASME Journal of Turbomachinery 111 (1989) 1–7.

[27] R.S. Abhari, A.H. Epstein, An experimental study of film cooling in a rotating transonic turbine, ASME Journal of Turbomachinery 116 (1994) 63–70.

[28] M.G. Dunn, C.W. Haldeman, Time-averaged heat flux for a recessed tip, lip, and platform of a transonic turbine blade, ASME Journal of Turbomachinery 122 (2000) 692–698.

[29] C.W. Haldeman, M.G. Dunn, Heat transfer measurements and predictions for the vane and blade of a rotating high-pressure turbine stage, ASME Journal of Turbomachinery 126 (2004) 101–109.

[30] S.J. Thorpe, S. Yoshino, R.W. Ainsworth, N.W. Harvey, An investigation of the heat transfer and static pressure on the over-tip casing wall of an axial turbine operating at engine representative flow conditions. (I) Time-mean results, Int. J. Heat and Fluid Flow 25 (2004) 933–944.

[31] S.J. Thorpe, S. Yoshino, R.W. Ainsworth, N.W. Harvey, An investigation of the heat transfer and static pressure on the over-tip casing wall of an axial turbine operating at engine representative flow conditions. (II) Time-mean results, Int. J. Heat and Fluid Flow 25 (2004) 945–960.

[32] D.H. Rhee, H.H. Cho, Local heat/mass transfer characteristics on a rotating blade with flat tip in a low speed annular cascade: Part 1.

Near-tip surface, ASME Journal of Turbomachinery 128 (2006) 96–109.

[33] D.H. Rhee, H.H. Cho, Local heat/mass transfer characteristics on a rotating blade with flat tip in a low speed annular cascade: Part 2. Tip and shroud, ASME Journal of Turbomachinery 128 (2006) 110–119.

[34] R.J. Goldstein, H.H. Cho, A review of mass transfer measurement using naphthalene sublimation, Experimental Thermal and Fluid Science 10 (1995) 416–434.

[35] S.J. Kline, F. McClintock, Describing uncertainty in single sample experiments, Mechanical Engineering 75 (1953) 3–8.

[36] E.R.G. Eckert, H. Sakamoto, T.W. Simon, The heat and mass transfer analogy factor, Nu/Sh, for boundary layers on turbine blade profiles, International Journal of Heat and Mass Transfer 44 (2001) 1223–1233.

[37] D.H. Rhee, Local heat/mass transfer characteristics on turbine rotor and shroud in a low speed annular cascade, PhD thesis, Yonsei University, Korea, 2004.

[38] J.P. Bindon, The measurement and formation of tip clearance loss, ASME Journal of Turbomachinery 111 (1989) 257–263.

[39] J. Moore, J.S. Tilton, Tip leakage flow in a linear turbine cascade, ASME Journal of Turbomachinery 110 (1988) 18–26.

[40] H.H. Cho, D.H. Rhee, J.H. Choi, Heat/mass transfer characteristics on turbine shroud with blade tip clearance, Annals of the New York Academy of Sciences 934 (2001) 281–288.